Shuttle High Resolution Accelerometer Package Experiment Results: Atmospheric Density Measurements Between 60 and 160 km

R. C. Blanchard*
NASA Langley Research Center, Hampton, Virginia
E. W. Hinson†
ST Systems Corporation, Hampton, Virginia
and
J. Y. Nicholson‡
Vigyan Research Associates, Inc., Hampton, Virginia

Indirect or inferred values of atmospheric density encountered by the Shuttle Orbiter during reentry are calculated from acceleration measurements made by the High Resolution Accelerometer Package (HiRAP) and the Orbiter inertial measurement unit (IMU) linear accelerometers. The atmospheric density data developed from this study represent a significant gain with respect to the body of data collected to data by various techniques in the altitude range of 60–160 km. The data are unique in that they cover a very wide horizontal range during each flight and provide insight into the actual density variations encountered along the re-entry flight path. The data, which were collected over a three-year period, are also characterized by variations in solar activity, geomagnetic index, and local solar time. Comparisons of the flight-derived densities with various atmospheric models show a significant wave-like variation with a constant wavelength, but whose phase is independent of altitude. The amplitude of this variation appears to have a dependence on solar activity and time of year. No statistically significant correlation could be established between this amplitude and geomagnetic activity or time of day for this data set.

Nomenclature

A_p = geomagnetic activity index
a = acceleration
C = aerodynamic force coefficient
F = force
$F_{10.7}$ = 10.7 cm solar flux
$\bar{F}_{10.7}$ = mean solar flux over three solar rotations centered on epoch
g = gravitational acceleration at sea level
Kn = Knudsen number, ratio of molecular mean free path to reference orbiter dimension of 32.7736 m (1290.3 in.)
L/D = lift to drag ratio
M = mass
R = ratio of normal to axial acceleration
S = area
t = time
V = velocity
$\bar{V}$ = viscous interaction parameter, $M(C/Re)^{1/2}$, where M, C, and Re are freestream Mach number, the Chapman-Rubesin proportionality constant, and Reynolds number, respectively
X,Z = HiRAP axes
X_b, Z_b = orbiter body axes
α = angle of attack
ΔC = change in C due to control surface deflection
ϵ = product of a_N/a_A and C_A/C_N
δ = control surface deflection angle
ρ = density (no subscript refers to measured density)
σ = standard deviation

Subscripts

A = axial
BF = body flap
C = continuum flow regime
D = drag
E = elevon
F = free molecule flow regime
L = lift
MSIS = Barnett and Corney/MSIS-83 atmosphere model
N = normal
X = component in X direction
Z = component in Z direction
76 = 1976 U.S. Standard Atmosphere model

Presented as Paper 88-0492 at the AIAA 26th Aerospace Sciences Meeting, Reno, NV, Jan. 11-14, 1988; received June 19, 1988; revision received Oct. 27, 1988.

*Senior Research Engineer, Aerothermodynamics Branch, Space Systems Division. Member AIAA.
†Chief Scientist.
‡Senior Research Engineer.

Introduction

ANALYSES of acceleration data from multiple flights of the Shuttle Orbiters have produced statistical refinement of the Orbiter aerodynamic model in the hypersonic rarefied flow regime.[1] Aerodynamic force coefficients cannot be determined in this flight regime by ground-based facilities; therefore, their preflight solutions have relied principally on computational techniques and engineering judgments.[2] These analyses and others conducted or sponsored by the Shuttle project have served to reduce the aerodynamic uncertainties through actual flight experience.[3] In turn, calculation of freestream atmospheric density from acceleration data can be

performed with a higher degree of certainty than previously possible.

Acceleration measurements have been obtained from the High Resolution Accelerometer Package (HiRAP) during 10 flights of orbiters OV-099 Challenger and OV-102 Columbia.[4] The HiRAP data have provided aerodynamically induced acceleration measurements from an altitude of 160 km in the near free molecule flow regime down to the range of 89–92 km.[5] These data have been combined with data from the inertial measurement unit (IMU) accelerometers to extend the data range down to 60 km in the hypersonic continuum regime, thereby spanning the entire transition region. Both accelerometer systems measure the components of the acceleration vector in the orbiter body axis system. The IMU accelerometers are used primarily for navigation and are 10^{-3} g instruments, whereas the HiRAP was designed specifically for aerodynamic research and resolves to the 1×10^{-6} g level. Inflight calibration of HiRAP for zero offset and temperature bias provides an accuracy of $2\text{–}10 \times 10^{-6}$ g.

The altitude range for HiRAP-IMU measurements, 60–160 km, coincides with the vertical region of the atmosphere where quality in situ data have been very sparse.[6] Previous measurements in this region have been limited to ground-based and vertical rocket probe techniques. Atmosphere models based on these data are generally mean vertical profiles with estimates of the extreme variation from the mean for latitudinal, annual, and solar activity effects. The acceleration-derived densities herein show the smaller scale dynamic variations over a wide range of altitudes and an even greater horizontal range. Comparison of the measured densities with standard atmosphere models indicates the presence of wave-like phenomena with amplitudes of up to $\pm 21\%$ relative to standard.

Experiment Description

The HiRAP experiment objectives, flight hardware, data reduction techniques, and earlier flight data analysis results are described in a series of earlier reports.[1,4,5,7,8] HiRAP was developed within the Orbiter Experiments (OEX) Project, which is conducting a broad spectrum of aerothermodynamic research during Shuttle ascent and descent. The acceleration data from HiRAP are intended to be combined with atmospheric density data from the Shuttle upper atmosphere mass spectrometer (SUMS)[9] for the extraction of aerodynamic coefficients in the hypersonic rarefield-flow regime.

The HiRAP is a system of three mutually orthogonal accelerometers of the gas-damped pendulous type and is mounted adjacent to the Aerodynamics Coefficient Identification Package (ACIP) with the HiRAP axes coincident with the orbiter body axis system. The individual accelerometers have a resolution of 1×10^{-6} g and a range of $\pm 8000 \times 10^{-6}$ g. The raw flight data samples (112 or 174 per second) are calibrated for bias and temperature sensitivity that are measured on each flight and for the effect of orbiter rotation about the body axes.[10] The data are then filtered to delete periods during attitude thruster firings and averaged over 1 s intervals.

The HiRAP data reduction produces a result that represents the aerodynamic acceleration signal plus any contribution from nonaerodynamic (impulsive) sources other than attitude thrusters. The major nonaerodynamic source identified to date is the auxiliary power unit (APU) exhaust, which produces a small thrust in the $+Z$ direction, equivalent to about 50×10^{-6} g. The Z-axis acceleration measurements are biased to account for the APU contribution, but the uncertainty in this bias is large compared with the aerodynamic signal at higher altitudes. The X-axis data are not affected and therefore used in the atmospheric density calculations at altitudes above 90 km. The HiRAP X-axis accelerometer saturates near 90 km, approximately 10 km below the Z-axis saturation point. The IMU Z-axis signal to noise ratio is acceptable below this altitude, and its data are used for atmospheric density calculations from there down to 60 km.

Experiment Concepts

Aerodynamic forces that affect stability, control, and structural design of flight vehicles are calculated for a given freestream density, velocity, and reference area by

$$F_i = \frac{1}{2} \rho V^2 C_i S$$

where C_i depends on the body shape and flow condition characterized by Knudsen number Kn in the rarefied flow regime. The value of C_i is usually determined for a given vehicle design by analytic techniques and/or wind-tunnel tests. These techniques have been developed to a high degree of accuracy for flight at low altitudes in the continuum flow regime.[11] At high altitudes in the free molecular flow, the forces are very small and usually of little concern in re-entry vehicle design. Problems arise, however, in the transition region between these limiting flow regimes where analytic and ground simulation are not yet accurate. The lack of knowledge and prediction technology in the transition region is the genesis for HiRAP and SUMS, and their objective is to fill this gap for the Shuttle Orbiter in particular and for winged re-entry vehicles in general.

The aerodynamic coefficients can be determined, if atmospheric density and vehicle acceleration are known, by rearranging the preceding force equation in the following manner:

$$C_i = \frac{2a_i}{\rho V^2 (S/M)}$$

where a_i is acceleration in the ith direction and S/M is the vehicle area to mass ratio. Substantial improvement in the knowledge of C_i depends on accurate simultaneous measurements of ρ and a_i. HiRAP is providing a_i, but ρ is not yet available from the SUMS experiment. Analysis of the HiRAP flight data has therefore been focused on obtaining the maximum amount of useful information from the data collected to date despite the lack of direct density measurements. Significant improvements to the orbiter aerodynamic model have been made possible by the large number of HiRAP flights. Increasing confidence in the model has encouraged its use in calculation of atmospheric density through the preceding relation, namely,

$$\rho = \frac{2a_i}{V^2 C_i (S/M)}$$

Aerodynamic Model Development

Background

The focus of the HiRAP flight data analysis has been on improvements to the orbiter aerodynamic model, specifically normal and axial force coefficients C_N and C_A. The absence of simultaneous freestream atmosphere density measurements with the acceleration measurements requires a statistical approach, which has been described in the literature at various stages of development. The model has evolved from the preflight aerodynamic design data base[12] to the current version based on all 10 flights of HiRAP. The model has been based on or influenced by various data from wind-tunnel tests, flight pressure measurements, flight acceleration measurements, and analytical studies, including the postflight aerodynamic assessment performed by the Shuttle Orbiter Project.[3]

Variation of Force Coefficients

The orientation of the resultant aerodynamic force vector in the orbiter body coordinate system at a given angle of attack depends on the aerodynamic flow properties that span the free molecule, transition, and hypersonic continuum flow regimes during orbiter re-entry. The force vector for $\alpha = 40$ deg is at an angular position near midway between the $-X_b$ and $-Z_b$ axes in free molecule flow as shown in Fig. 1. The vector

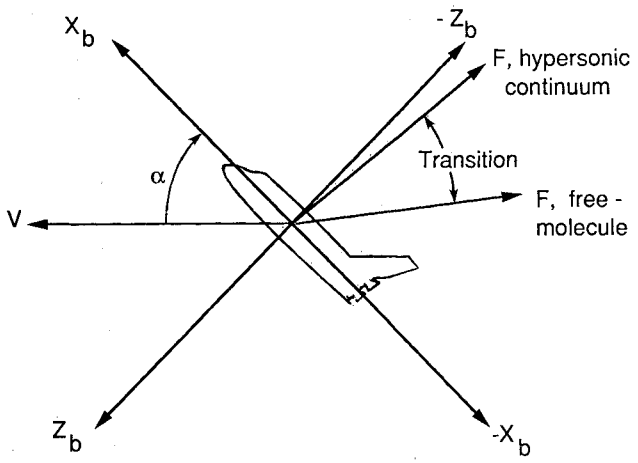

Fig. 1 Orbiter flight geometry during re-entry.

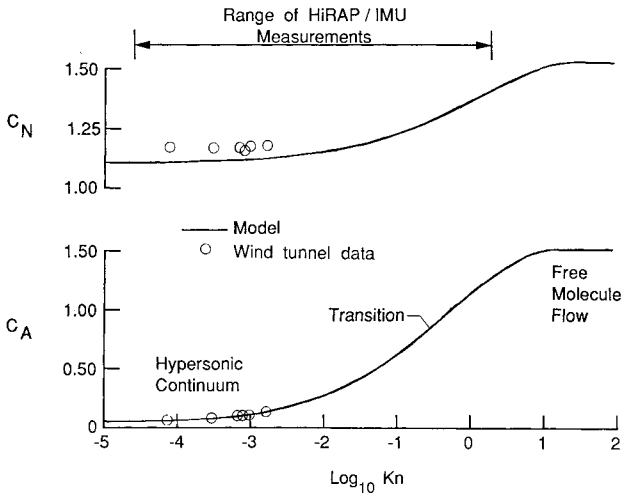

Fig. 2 Variation of normal and axial force coefficients.

moves from this position in the direction of the $-Z_b$ axis as transition begins and stops at a point just aft of the $-Z_b$ axis when the hypersonic continuum is reached. The normal force coefficient C_N is determined by the projection of the vector on the Z_b axis; likewise, the axial force coefficient C_A is determined by the projection on the X_b body axis. The ratio of coefficients C_N/C_A is equal to the ratio of acceleration (or force) measured along Z_b and X_b axes a_z/a_x and is independent of atmospheric density on either side of the transition region. The aerodynamic flow properties and the resultant orientation of the force vector are dependent on Kn, the ratio of molecular mean free path to a vehicle reference length, in the transition region and are therefore dependent on density. The variations of C_N and C_A with Kn are shown in Fig. 2 for the current model at $\alpha = 40$ deg and $\delta_E = \delta_{BF} = 0$ deg. Included in Fig. 2 are wind-tunnel data taken from a 1% scale model in a hypersonic shock tunnel facility by the Orbiter Project early in the program.[2] The objective of the tests was to explore viscous interaction effects; therefore, the tests were conducted at large Mach numbers (up to 16) and viscous interaction parameter V values (up to 0.06). Clearly, viscous effects for the orbiter at an angle of attack of 40 deg were accounted for quite adequately; i.e., C_N is insensitive, while C_A shows a marked increase resulting from increased shear. However, there is an apparent shift in C_N wind-tunnel data with respect to the flight-derived model shown. This shift may be caused by the real gas effects discovered through study of the pitching moment behavior after the first flight of the orbiter.[11] The explanation is that wind-tunnel data must be adjusted (C_N lowered in value by about 6%) due to lower pressures on the aft part of the orbiter.[13] This provides excellent agreement with the C_N model derived from multiple flights of the HiRAP/IMU. It is suggested that C_A also increases by about 6% because of real gas effects, but the C_A model derived from the flight data does not support this, as seen in Fig. 2.

C_N and C_A vary significantly with angle of attack and to a much lesser extent with the deflection angles of the elevon and body flap. The model treats the continuum and free molecule flow values of C_N and C_A as asymptotes defined as functions of α, δ_E, and δ_{BF} as follows:

$$(C_N)_C = (C_{N_\alpha})_C + (C_{N_E})_C + (C_{N_{BF}})_C$$

$$(C_N)_F = (C_{N_\alpha})_F + (C_{N_E})_F + (C_{N_{BF}})_F$$

$$(C_A)_C = (C_{A_\alpha})_C + (C_{A_E})_C + (C_{A_{BF}})_C \text{ and}$$

$$(C_A)_F = (C_{A_\alpha})_F + (C_{A_E})_F + (C_{A_{BF}})_F$$

These values are then connected by a bridging formula that spans the transition region between the limiting flow conditions on either side as follows:

$$C_N = (C_N)_c + [(C_N)_F - (C_N)_c]\bar{C}_N$$

and

$$C_A = (C_A)_c + [(C_A)_F - (C_A)_c]\bar{C}_A$$

where

$$\bar{C}_N = \exp\left(-A\,|B - \log_{10}Kn\,|^C\right)$$

and

$$\bar{C}_A = \exp\left(-D\,|E - \log_{10}Kn\,|^F\right)$$

The model has been developed by defining the asymptotic values $(C_N)_c$, $(C_N)_F$, $(C_A)_c$, and $(C_A)_F$, based on all available data and then solving for the bridging formula coefficients, A-F, that best fit the acceleration data obtained from the orbiter flights.[8]

Development Technique

Previous studies of the HiRAP flight data have used the orbiter lift-to-drag ratio, L/D, as an aid to aerodynamic model development. Flight measurements of L/D are obtained from the function

$$L/D = \frac{R - \tan\alpha}{1 + R\tan\alpha}$$

where R is the measured Z to X (normal to axial) acceleration ratio at angle of attack, α. This gives a near atmosphere-density-independent (when averaged over many flights) measure of the ratio of lift coefficient to drag coefficient C_L/C_D. The average L/D for 10 HiRAP flights has served as the statistical basis for determination of C_N and C_A by fitting L/D derived from the aerodynamic model to the flight-measured average. However, examination of the preceding equation reveals a limitation with the use of L/D as a fitting criterion and as a reference for comparison of different data sets such as flight measurements, wind-tunnel measurements, and analytic calculations. The ratio R becomes large as the flow transitions toward the hypersonic continuum such that L/D approaches a limit depending on α and becomes insensitive to variations in R. Consequently, any differences between data sets will be suppressed in that region leading to an unrealistic comparison between data sets. Conversely, using L/D as a model-fitting criterion in this region results in magnification of small L/D errors into large errors in the ratio C_N/C_A.

A better fit of the aerodynamic model in terms of C_N/C_A at the continuum end of transition can be obtained by direct comparison of C_N/C_A with the measured acceleration ratio a_N/a_A. The lower graph on Fig. 3 shows a comparison of the average a_N/a_A ratio for 10 HiRAP flights with the C_N/C_A values from the aerodynamic model derived in this study. Included on the figures are the previously discussed wind-tunnel data to which earlier models were fitted based on L/D. The need for improvement in the earlier models is clearly indicated in the a_N/a_A curves, whereas such a need is hardly detectable in an L/D comparison. A quantitative measure of the model fit to the flight measurements can be seen more vividly in the upper graph in Fig. 3 where the parameter $\epsilon = (a_N/a_A)\cdot(C_A/C_N)$ is shown. This product should be unity if the aerodynamic model is correct and the acceleration measurements are accurate. Requiring that the product be unity is equivalent to the requirement for consistency between the equations for C_N and C_A and the ratio of the flight-measured accelerations, or in other words, the density derived from both X and Z channels must be equal.

Since the measured acceleration ratio only gives the ratio of C_N to C_A, some logical criteria must be applied to fix one of the coefficients in both the continuum and free molecule flow regimes. No firm criteria were defined for the free molecule flow regime, so both C_N and C_A were varied from the initial Orbiter Design Data Book[12] values to match the flight measured acceleration ratio. The continuum C_N was fixed according to the Orbiter Design Data Book initially, then to early HiRAP flight results, and finally to flight pressure measurements from the latest mission, STS-32. The STS-32 mission was the first flight for the Shuttle Entry Air Data System (SEADS),[14] which measures surface pressure at the port shared with SUMS just aft of the stagnation point at reentry attitude. Atmosphere densities were derived from these pressure data with the aid of a pressure coefficient model that is based on a real-gas solution confirmed by flight measurement[15] in the continuum regime. The continuum value for the pressure coefficient is tied to Monte Carlo direct simulation solutions[9] in the upper transition region (above 95 km) and the free molecule flow regime. The densities obtained from the pressure measurements using this pressure coefficient model were normalized to the 1976 U.S. Standard Atmosphere model[16] as shown in Fig. 4, which also shows for comparison the acceleration-derived densities for the aerodynamic model. The difference between the two solutions above 70 km results from pressure coefficient model limitations in the lower transition region. The continuum C_N for the aerodynamic model based on the flight pressure measurements has a value consistent with wind-tunnel data corrected for real-gas effects, which matches the orbiter postflight update within 3%, and which produces a 10-flight average of acceleration derived densities much closer to the mean atmosphere models at 60–70 km.

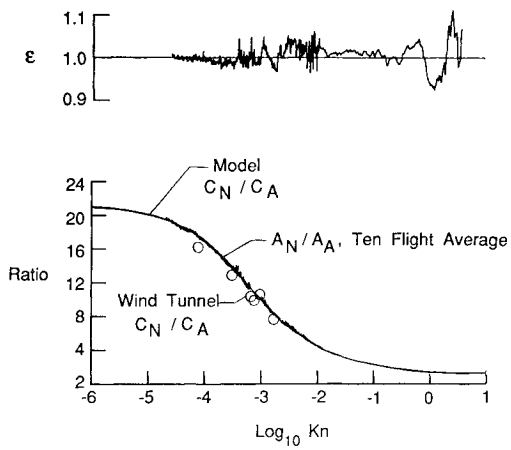

Fig. 3 Aerodynamic model compared with measurements.

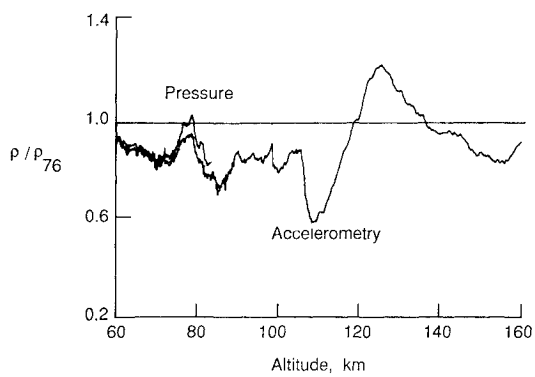

Fig. 4 Comparison of accelerometry and pressure derived densities from STS-32.

Model Update

This latest analysis of the HiRAP flight data has resulted in three improvements to the aerodynamic model. The value of $(C_A)_c$ was reduced about 5%, which moves the model closer to the orbiter postflight update value. This change yields a better fit to the flight data in the lower transition region, 60–70 km. The preflight function for $(\Delta C_A)_E$ in the continuum region produced large (up to 10%) errors in the C_N/C_A ratio compared to flight measurements of a_N/a_A for negative elevon deflection angles. This error is removed by reducing the elevon effectiveness to one-third of the preflight value when $\delta_E < 0$ deg. The flight-measured acceleration ratio indicates a decrease in $(C_A)_F$ of 5% is necessary to obtain a good fit in the upper transition region, 100–120 km.

Atmospheric Density Measurements

Coverage

The inferred atmospheric densities derived from the HiRAP and Orbiter IMU are unique in that they cover a region of the atmosphere where measurement has been sparse historically. Some measurements of temperature and estimates of pressure and density have been made in this region (60–160 km), but the density estimates have large uncertainties. Those data have been primarily vertical profiles obtained from small sounding rocket programs that have recently been discontinued. The Shuttle measurements herein have the advantage of covering a very wide horizontal range and therefore may provide some insight into the latitudinal, longitudinal, and local solar time variations of density. The measurements in the range of 80–120 km may also provide some insight into the transition from eddy mixing to molecular diffusion.

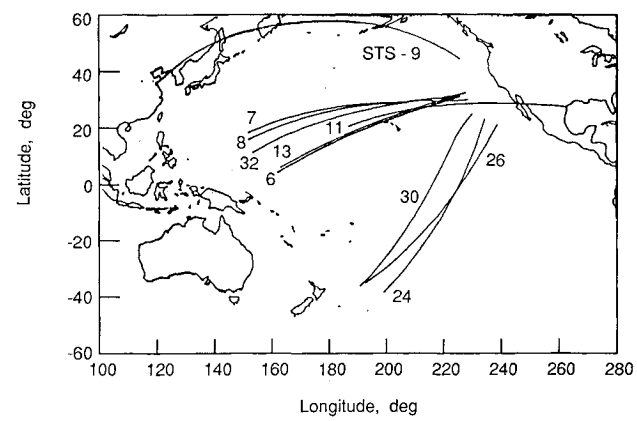

Fig. 5 Entry ground tracks of STS 6, 7, 8, 9, 11, 13, 24, 26, 30, and 32 from 160–60 km.

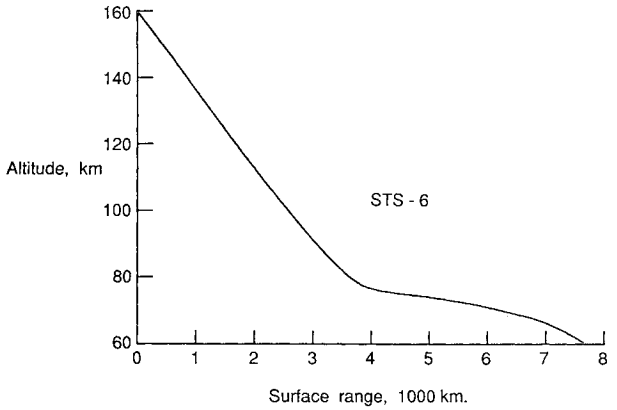

Fig. 6 Typical spatial coverage during Shuttle re-entry.

Additionally, the newly acquired density data should provide models with variations in the critical 80–120 km region, a regime where lower atmosphere models merge with the upper atmosphere models. Lower altitude models vary with latitude and time of year only. However, above 120 km, models have been developed based upon satellite drag densities and mass spectrometer measurements. These models characteristically use diffusive equilibrium assumptions and special spherical harmonic techniques to account for many variables such as latitude, longitude, local solar time effects, and solar and geomagnetic activity. To connect the upper and lower models requires assumptions on the variability of density with respect to these model parameters. The density measurements provided by the HiRAP experiment may provide the appropriate insight in the connecting region to realistically account for these variations.

The 10 HiRAP flights from April 1983 to January 1986 have spanned a wide variation of the parameters known to

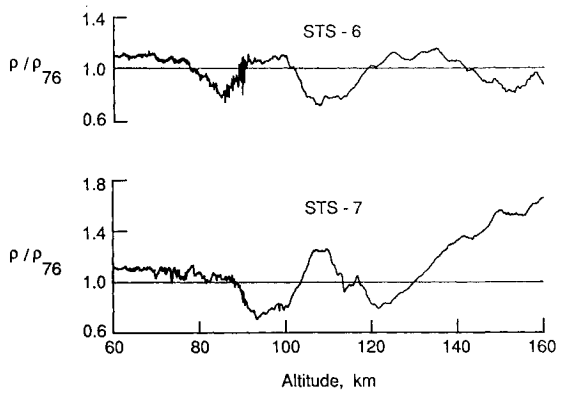

a) STS-6 and STS-7

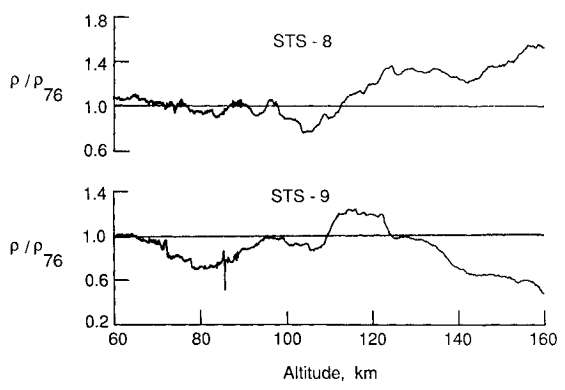

b) STS-8 and STS-9

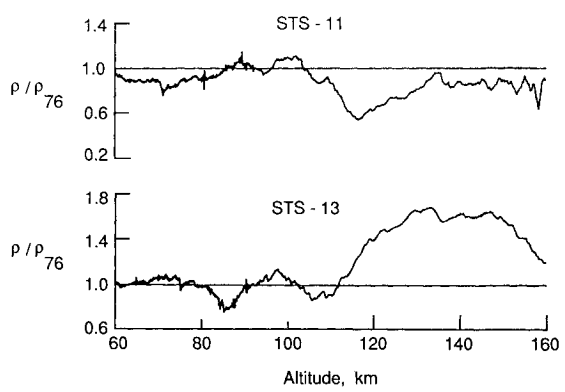

c) STS-11 and STS-13

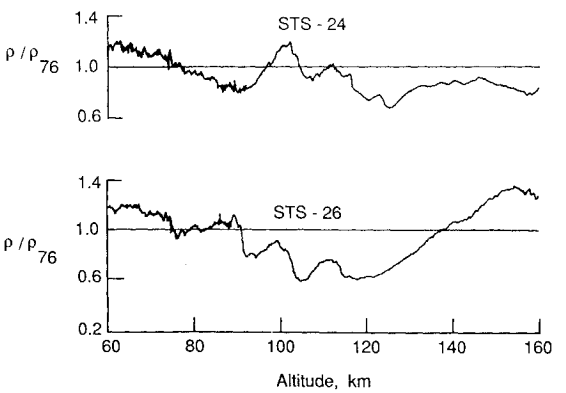

d) STS-24 and STS-26

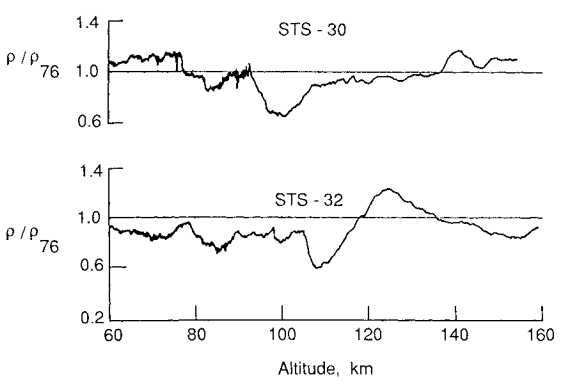

e) STS-30 and STS-32

Fig. 7 Density measurements normalized to U.S. 76 Standard Atmosphere.

influence atmospheric density. The ground track coverage in terms of latitude and longitude during re-entry is shown in Fig. 5. Three flights approach the landing site on a southern latitude track, six on a mid-northern latitude track, and one from high-northern latitudes. Figure 6 shows the typical relationship between altitude and surface range along the orbiter flight path. Flight-to-flight variations from this profile are small because of very rigid constraints on the reentry trajectory. With respect to local solar time, four flights re-entered during total darkness, and two re-entered during total daylight. Three flights crossed the morning terminator going from night to day, whereas one flight crossed the evening terminator going from day to night.

The 10.7 cm solar flux for the 10 flights spans the range of low solar activity up to moderate activity. The 10.7 cm solar radiation incident at the Earth's surface is used as an indicator of solar activity effect on the atmosphere even though the wavelength associated with most ionizations and chemical reaction initiations is of the order of 2×10^{-5} cm. The 10.7 cm measurement is a widely accepted indicator of the flux in the ultraviolet region and correlates well with observed variations in atmospheric density. Atmosphere models use the previous day measure of the solar flux and the 81 day (three solar rotations) average centered on the epoch to account for the complex and dynamic effects that chemistry has on density.

Geomagnetic activity index A_p varied from 3–22, which is considered to be in the range of quiet to typical. The parameter A_p is relatively important at altitudes around 120 km and therefore should influence the density measurements in the range 90–140 km.[17] Finally, the distribution of HiRAP flights as a function of time of year is fairly uniform, and a significant annual or semi-annual effect could be detectable.

Atmosphere Density Results

Atmosphere densities have been calculated over the altitude range of 60–160 km during re-entry for the STS-6, 7, 8, 9, 11, 13, 24, 26, 30, and 32 Shuttle flights. The density profiles were normalized to the 1976 U.S. Standard Atmosphere model as shown in Figs. 7a–e. The choice of altitude as abscissa for these plots is rather arbitrary, and it should be emphasized that unlike sounding rocket data, a large horizontal range is also covered over this altitude span. Examination of these plots shows a pattern of wavelike structure with amplitudes up to ±21% relative to standard and peak-to-peak altitude increments of about 35 km, equivalent to about 1800 km horizontal distance. These waves appear to be somewhat random, in that maxima occur at different altitudes and the wave amplitude varies from flight to flight. This observation is essentially confirmed in the 10-flight average of ρ/ρ_{76} shown in Fig. 8. Some structure remains in the average, but the amplitude and wavelength are both substantially less than in the individual cases. A larger data sample would most likely remove this residual structure altogether.

The derived densities were also normalized to two other atmosphere models: 1) the Jacchia 1970 model coded at NASA Marshall Space Flight Center, MSCF/J70,[18] and 2) a combination model employing a middle atmosphere (60–80 km) reference model by Barnett and Corney[19] and the MSIS-83 model[6] above 90 km with interpolation between 80 and 90 km. The ρ/ρ_{model} for 10 flights for each of these models was also averaged, and the results are shown with those from the 1976 U.S. standard for comparison in Fig. 9. The MSFC/J70 model only applies to altitudes above 85 km and closely matches the 1976 U.S. standard from that altitude up to 110 km, beyond which differences of up to 10% occur. The MSIS-83 model generally parallels the 1976 U.S. standard to about 110 km, where it diverges rather dramatically, with differences up to 30%. All the models predict the large-scale variation of density fairly well on the average, but none of the three predicts the smaller scale wave structure appearing in the individual flights. The 1976 U.S. Standard Atmosphere represents a mean model that depends on altitude alone. The MSIS-83 model and the MSFC/J70 models are complete global models in the sense that all of the known variables having a significant influence on atmosphere density are incorporated (solar flux, geomagnetic activity, altitude, latitude, longitude, local solar time, and annual/semi-annual effects). The envelope of variation of the Barnett and Corney/MSIS-83 model with respect to the 1976 U.S. standard along the tracks of the 10 Shuttle flights is shown in Fig. 10 and indicates the differences between the models. Also shown in Fig. 10 is the envelope for ρ/ρ_{76} with the much greater variability of the actual atmosphere density being obvious at higher altitudes. This result is expected because the models produce mean density values based on past observations in this altitude range where atmospheric dynamics have been neither well understood nor well measured. The rather large spread between the maximum and minimum $\rho_{\text{MSIS}}/\rho_{76}$ of 60 and 80 km in Fig. 10 results

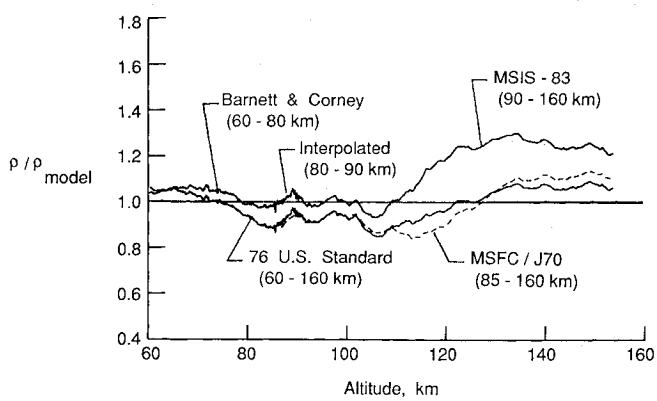

Fig. 9 Comparison of average measured density normalized to various atmosphere models.

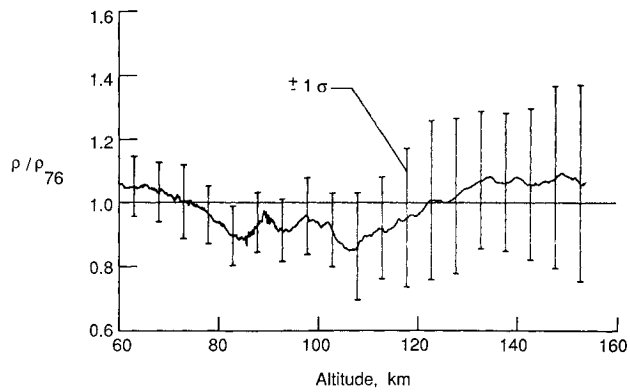

Fig. 8 Average normalized density measurements for 10 HiRAP flights.

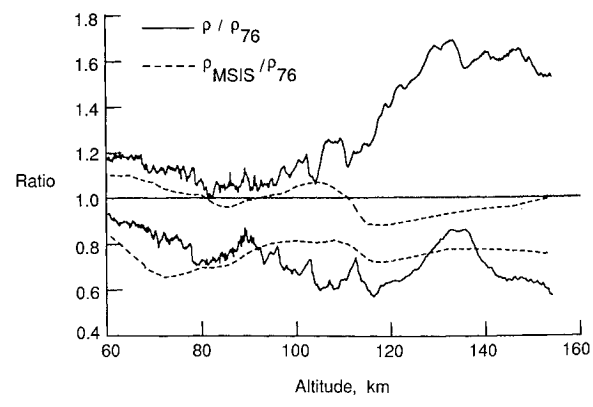

Fig. 10 Envelope of maximum and minimum density ratios.

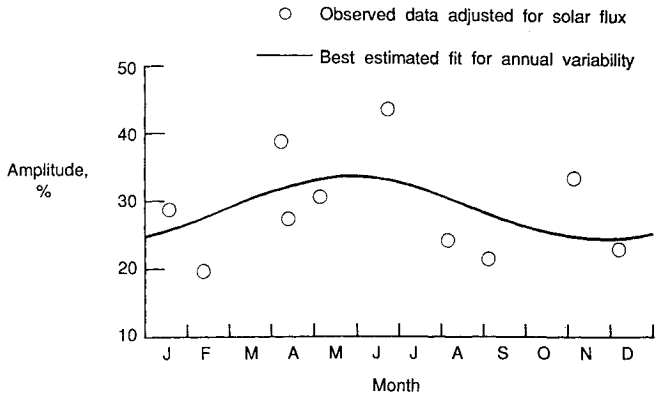

Fig. 11 Annual variability in the amplitude of the normalized density (ρ/ρ_{76}) between 80 and 115 km.

from the extreme northerly track of STS-9 during re-entry. Omitting STS-9 produces an envelope for ρ_{MSIS}/ρ_{76} with less than one-half of the spread in that altitude range, highlighting the strong latitudinal dependence of the Barnett and Corney model.

The cause of the wave structure seen in the individual flights has not been definitely determined. The obvious possibility that the observed wave patterns are caused by variation in horizontal or vertical wind speeds was rejected essentially because such high wind speeds are required, on the order of several hundred meters per second, to produce such density variations. If the variations are temporal, their fluctuations are too rapid to be caused directly by slowly varying influences such as A_p, $F_{10.7}$, time of year, or even local solar time. However, these variables could influence the mechanisms that produce the waves and thereby indirectly influence both their temporal and spatial dependence, as well as their amplitude.

Correlation studies were undertaken to determine if the nature of these waves did depend on any of the variables listed previously. The waves appear to be completely random with respect to altitude; i.e., essentially no spatial dependence with any of the variables was observed. In order to determine their temporal and amplitude dependence, the amplitude of each wave pattern was found by fitting the ρ/ρ_{76} data for each flight between 80 and 115 km to a straight line with a superimposed sine wave in which frequency was allowed to vary. The frequency of each sine wave was found to be fairly constant, about 0.004 s^{-1}, corresponding to 250 s or approximately 37 km altitude change and 1850 km horizontal range. The peak-to-peak amplitude result for each flight was divided by its average ρ/ρ_{76} ratio to give a percentage change. In turn, the percentage changes were correlated with time of year, A_p, $F_{10.7}$, and the deviation of $F_{10.7}$ from its mean ($F_{10.7} - \bar{F}_{10.7}$) by estimating the changes with an expansion including these quantities. The residuals (observations minus estimates) of all 10 flights were minimized by the method of least squares, and the coefficients for all quantities along with their respective errors were calculated. The coefficients for A_p and $F_{10.7} - \bar{F}_{10.7}$ were found to be statistically insignificant, and the process was repeated without them. The results showed that the amplitude of the annual component, its phase, and the $F_{10.7}$ dependence have 1σ errors fewer than the coefficients. Figure 11 shows the observations corrected for the $F_{10.7}$ effect (approximately + 0.1% change per $F_{10.7}$ unit) along with a plot of the time of year (annual) effect. Unfortunately, most of the Shuttle re-entry data are confined to a 12-hour period (only one exception), and no meaningful correlation could be estimated with local solar time. It is hoped that future Shuttle flights will yield data at local solar times not experienced to date, and this correlation can be established.

Several possible types of waves might have caused this small-scale wave structure. Perhaps the most likely candidates are gravity waves. These could produce the vertical structure observed, and evidence suggests that the extent of gravity wave production and/or propagation into the transition region is seasonally dependent.[20] In order for gravity waves to be a valid explanation, it would be necessary for their horizontal coherence to exist over 1850 km, the horizontal distance covered by the Orbiter during one cycle.

Conclusions

Acceleration data obtained during 10 flights of the Shuttle Orbiter have made possible significant improvement in the orbiter aerodynamic model for normal and axial force coefficients. The HiRAP experiment has provided flight acceleration data at higher altitudes than previously possible and has facilitated the statistical determination of force coefficients in the transition region. These improvements in the aerodynamic model have made possible the calculation of inferred atmospheric densities with a high degree of confidence.

Atmosphere densities, when compared with current atmosphere models, show significant variations of a wave-like character that appear to be random from flight to flight. The wavelength appears to be fairly constant (approximately 37 km in altitude), but the amplitude shows indications of an annual dependence with maxima near the solstices. Phasing of the waves with respect to altitude is random. Variation of measured densities from current atmosphere models is large (in excess of 50%) for the individual flights, but these differences are diminished in the average of 10 flights.

References

[1]Buck, G. M. and Blanchard, R. C., "Rarefied Aerodynamics and Upper Atmosphere Density from Multiple Orbiter Flight Measurements," AIAA Paper 86-0269, Jan. 1986.

[2]"Aerodynamics Design Substantiation Report—Vol. I: Orbiter Vehicle," Rockwell International, Space Division, Downey, CA, SD74-SH-0206-1H, Jan. 1975.

[3]Romere, P. O., "Flight Assessment Package Orbiter Aerodynamics, FAD-26," JSC-22078, April 1986.

[4]Blanchard, R. C. and Larman, K. T., "Rarefied Aerodynamics and Upper Atmospheric Flight Results from the Orbiter High Resolution Accelerometer Package Experiment," AIAA Paper 87-2366, Aug. 1987.

[5]Blanchard, R. C. and Rutherford, J. F., "Shuttle Orbiter High Resolution Accelerometer Package Experiment: Preliminary Flight Results," *Journal of Spacecraft and Rockets,* Vol. 22, July-Aug. 1985, pp. 474-480.

[6]Hedin, A. E., "A Revised Thermospheric Model Based on Mass Spectrometer and Incoherent Scatter Data: MSIS-83," *Journal of Geophysical Research,* Vol. 88, Dec. 1983, pp. 10170-10188.

[7]Blanchard, R. C., and Buck, G. M., "Rarefied-Flow Aerodynamics and Thermosphere Structure from Shuttle Flight Measurements," *Journal of Spacecraft and Rockets,* Vol. 23, Jan.-Feb. 1986, pp. 18-24.

[8]Blanchard, R. C., "Rarefied Flow Lift-to-Drag Measurements of the Shuttle Orbiter," *Proceedings of the 15th Congress of International Council of Aeronautical Sciences,* Vol. 2, Paper ICAS-86-2.10.2, London, Sept. 1986, pp. 1421-1430.

[9]Blanchard, R. C., Duckett, R. J., and Hinson, E. W., "A Shuttle Upper Atmosphere Mass Spectrometer (SUMS) Experiment," *Journal of Spacecraft and Rockets,* Vol. 21, Mar. 1984, pp. 202-208.

[10]Thompson, J. M., Russell, J. W., and Blanchard, R. C., "Methods for Extracting Aerodynamics Accelerations from Orbiter High Resolution Accelerometer Package Flight Data," AIAA Paper 87-2365, Aug. 1987.

[11]Romere, P. O., Kanipe, D. B., and Young, J. C., "Space Shuttle Entry Aerodynamics Comparisons of Flight with Preflight Predictions," *Journal of Spacecraft and Rockets,* Vol. 20, Jan.-Feb. 1983, pp. 15-21.

[12]Aerodynamic Design Data Book—Vol. I: Orbiter Vehicle, NASA CR-160386, 1978.

[13]Maus, J. R., Griffith, B. J., Szema, K. Y., and Best, J. T., "Hypersonic Mach Number and Real-Gas Effects on Space Shuttle Orbiter Aerodynamics," *Journal of Spacecraft and Rockets,* Vol. 21, Mar.-Apr. 1984, pp. 136-141.

[14]Siemers, P. M. III, Wolf, H., and Flanagan, P. F., "Shuttle Entry Air Data System Concepts Applied to Space Shuttle Orbiter Flight Pressure Data to Determine Air Data—STS 1-4," AIAA Paper 83-0118, Jan. 1983.

[15]Weilmuenster, K. J. and Hamilton, H. H. II, "A Comparison of Computed Space Shuttle Orbiter Surface Pressures With Flight Measurements," AIAA Paper 82-0937, June 1982.

[16]"U.S. Standard Atmosphere, 1976," U.S. Government Printing Office, Washington, DC, 1976.

[17]Mays, H. G. and Vollard, H., "Magnetic Storm Characteristics of the Thermosphere," *Journal of Geophysical Research,* Vol. 78, May 1973, pp. 2251-2264.

[18]Johnson, Dale L. and Smith, Robert E., "The MSFC/J70 Orbital Atmosphere Model and the Data Bases for the MSFC Solar Activity Prediction Technique," NASA TM 86522, Nov. 1985.

[19]"Middle Atmosphere Program," *Handbook for MAP, Volume 16,* edited by K. Labitzke, J. J. Barnett, and B. Edwards, U.S. Government Printing Office, Washington, DC, July 1985, pp. 47-85.

[20]Fritts, D., "Upper and Middle Atmospheric Density of Modeling Requirements for Spacecraft Design and Operations," NASA CP-2460, Nov. 1985, pp. 245-248.